Journal of South American Earth Sciences 52 (2014) 43–56

Contents lists available at ScienceDirect

Journal of South American Earth Sciences

journal homepage: www.elsevier.com/locate/jsames

Syn- and post-sedimentary controls on clay mineral assemblages in a tectonically active basin, Andean Argentinean foreland

Margarita Do Campo [a,*], Fernando Nieto [b], Cecilia del Papa [c], Fernando Hongn [d]

[a] INGEIS (CONICET – Universidad de Buenos Aires) y FCEyN, U.B.A. Pabellón INGEIS, Ciudad Universitaria, 1428 Buenos Aires, Argentina
[b] Departamento de Mineralogía y Petrología and I.A.C.T., Universidad de Granada – CSIC, Avda. Fuentenueva s/n, 18002 Granada, Spain
[c] CICTERRA, CONICET – Universidad Nacional de Córdoba, Córdoba, Argentina
[d] IBIGEO (CONICET – Universidad Nacional de Salta), Avda. Bolivia 5150, 4400 Salta, Argentina

ARTICLE INFO

Article history:
Received 7 February 2013
Accepted 21 December 2013

Keywords:
Foreland basins
Diagenesis
Illite/smectite mixed-layers
Kaolinite
NW Argentina

ABSTRACT

In the northern part of the Calchaquí Valley (NW Argentina), Palaeogene Andean foreland sediments are represented by a 1400-metre-thick continental succession (QLC: Quebrada de Los Colorados Formation) consisting of claystones, siltstones, sandstones, and conglomerates representing sedimentation in fluvial-alluvial plains and alluvial fan settings. To understand the main syn- and postsedimentary variables controlling the clay mineral assemblages of this succession, we have studied the fine-grained clastic sediments by X-ray diffraction and electron microscopy, along with a detailed sedimentary facies analysis, for two representative sections. In the northern section, the whole succession was sampled and analysed by XRD, whereas in the second section, a control point 15 km to the south, only the basal levels were analysed. The XRD study revealed a strong contrast in clay mineral assemblages between these two sections as well as with sections in the central Calchaquí Valley studied previously. In the northernmost part of the study area, a complete evolution from smectite at the top to R3 illite/smectite mixed-layers plus authigenic kaolinite at the bottom, through R1-type mixed-layers in between, has been recognized, indicating the attainment of late diagenesis. In contrast, the clay mineral assemblages of equivalent foreland sediments cropping out only 15 km to the south contain abundant smectite and micas, subordinate kaolinite and chlorite, and no I/S mixed-layers to the bottom of the sequence. Early diagenetic conditions were also inferred in a previous study for equivalent sediments of the QLC Formation cropping out to the south, in the central Calchaquí Valley, as smectite occurs in basal strata. Burial depths of approximately 3000 m were estimated for the QLC Formation in the central and northern Calchaquí Valley; in addition, an intermediate to slightly low geothermal gradient can be considered likely for both areas as foreland basins are regarded as hypothermal basins. Consequently, the attainment of late diagenesis in the northernmost study area cannot be explained by significant differences in burial depth nor in geothermal gradient in relation to the section 15 km to the south nor with the central Calchaquí Valley. The formation of R3 mixed-layer I/S and authigenic kaolinite in the northern study area was most likely controlled by the circulation of hot, deep fluids along the reverse faults that bounded the Calchaquí valley. These faults were active during the Cenozoic, as evidenced by the syndepositional deformation features preserved in the studied sediments. Stress could also have been a driving force in burial diagenesis at the R3 mixed-layer I/S stage in these young continental sediments.

1. Introduction

Variations in the clay mineral assemblages of ancient deposits have been successfully employed to investigate long-term trends in provenance and palaeoclimate of a variety of sedimentary successions all over the world (Adatte et al., 2002; Fagel et al., 2003; Suresh et al., 2004; Dera et al., 2009). Depending on the interplay of several variables including climate, tectonics, source area lithology, and burial history, sediments can contain clay minerals of detrital or diagenetic (neoformed and/or transformed) origin. Detrital clay minerals are derived directly from the weathering of crystalline rocks in the basin and drainage areas, but can also be recycled from ancient sedimentary rocks. In successions that have not been buried deeply, variations in clay-mineral assemblages are frequently employed to reconstruct palaeoclimatic changes, based upon the premise that the other variables play a secondary role

* Corresponding author. Tel.: +54 114783 3021.
E-mail addresses: docampo@ingeis.uba.ar (M. Do Campo), nieto@ugr.es (F. Nieto), delpapacecilia@yahoo.com (C. del Papa), Fhongn@aol.com (F. Hongn).

0895-9811/$ – see front matter © 2014 Elsevier Ltd. All rights reserved.
http://dx.doi.org/10.1016/j.jsames.2013.12.008

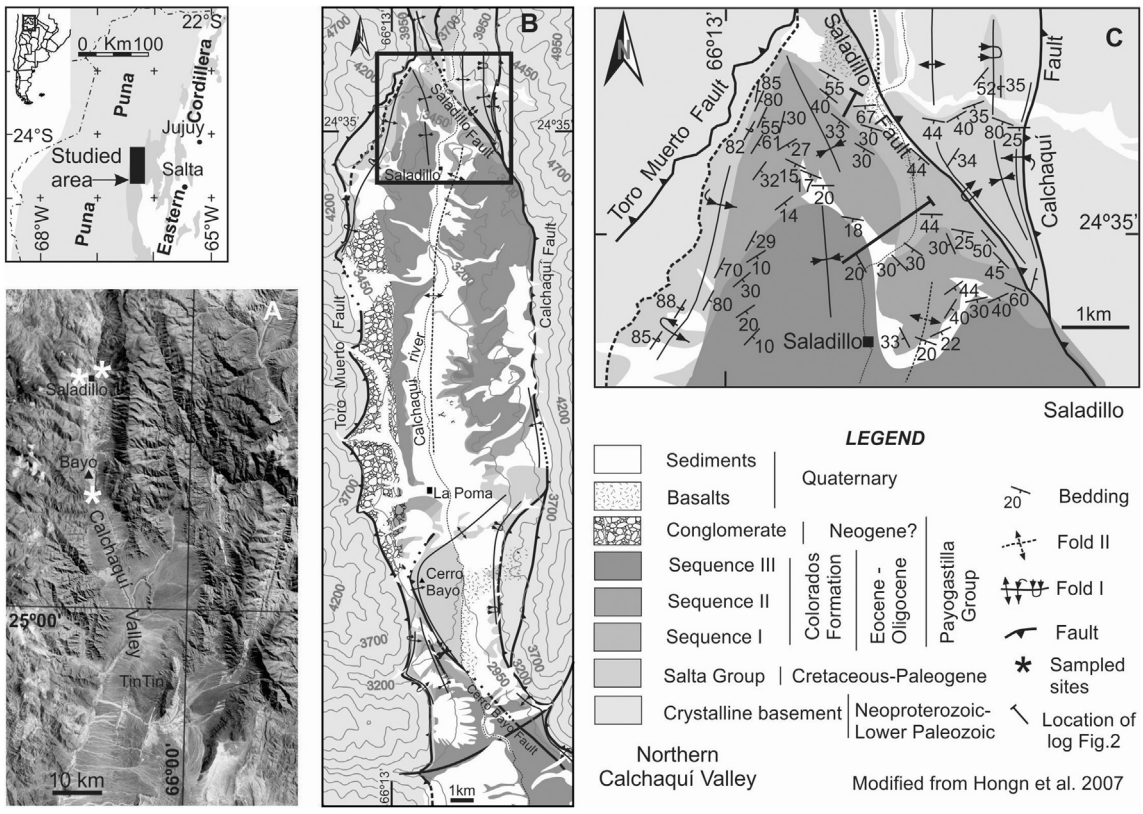

Fig. 1. A) Satellite image of the northern Calchaquí Valley, sampling sites (Saladillo and Cerro Bayo) are shown. The location of Tin Tin basin, previously studied by Do Campo et al. (2010), is also shown. B) Location and geological map of the northern Calchaquí Valley. C) Detailed geological map of the Saladillo area and location of stratigraphic log described in Fig. 2.

(Adatte et al., 2002; Saèz et al., 2003; Suresh et al., 2004; Fesharaki et al., 2007). In this context, Chamley (1989) proposed the kaolinite/muscovite ratio (Kln/Ms) as a palaeoclimatic indicator taking into account that fined-grained white mica represents a product of predominantly physical weathering typical of dry climates, whereas kaolinite formation is favoured by wet climates and requires a minimum temperature of 15 °C (Adatte et al., 2002). However, such approaches must be used with caution because clay minerals can only be used as a palaeoclimatic proxy when they derive from mature and mineralogically differentiated soils formed during the same sedimentary cycle (Thiry, 2000). Furthermore, in active settings, tectonism can change the dominant composition of the detritus carried to the basin since it can modify continental morphology and produce changes in source areas.

On the other hand, when the clay assemblages are modified by diagenetic reactions, clay minerals are useful to constrain a basin's thermal history (Dorsey et al., 1988; Arostegui et al., 2006; Collo et al., 2011). The transformation of smectite to illite through illite/smectite (I/S) mixed-layers is one of the main mineral reactions during the burial diagenesis of mudstones (Merriman and Peacor, 1999). This transformation has received considerable attention since the mid-seventies not only due to academic interest but also because it is closely associated with the initial steps of hydrocarbon generation and its subsequent migration (e.g. Pollastro, 1993). Consequently, numerous research papers have attempted to correlate the state of reaction progress of the smectite-I/S-illite series with burial temperature and also with organic indicators of basin maturity, such as vitrinite reflectance (Bevins et al., 1996; Arostegui et al., 2006).

Even though the study of clay mineral assemblages in conjunction with facies analysis has been established as a powerful tool in basin analysis, this approach has been little used so far to decipher the complex history of Andean foreland basins (Net et al., 2002; Do Campo et al., 2010; Collo et al., 2011). As foreland basins receive synorogenic sediments from fold-thrust belts, understanding their sedimentary and tectonic evolution could contribute to understanding the history of the orogen itself.

As part of an extensive study on the evolution of Palaeogene Andean foreland basins in NW Argentina, we have undertaken a study of clay-mineral assemblages applying XRD, SEM, and detailed sedimentary facies analysis for three representative sections in the northern (Saladillo and Cerro Bayo areas) and central Calchaquí Valley (Tin Tin basin, Fig. 1). The results of the mineralogical and sedimentological study of a 1400-metre-thick Palaeogene succession of the Tin Tin basin had been presented in a previous contribution (Do Campo et al., 2010). In that area, smectite occurs in the basal siltstones of the foreland sediments, thereby suggesting early diagenesis for the entire sequence, in agreement with the burial depths of ~3000 m estimated for the sediment column. In contrast, in the northernmost part of the Calchaquí Valley, a preliminary study evidenced I/S mixed-layers in the basal levels (Do Campo et al., 2008), indicative of late diagenesis. Moreover, the XRD study revealed a strong contrast in kaolinite abundances between the central and northern regions of the Calchaquí Valley. The present study has focused on the clay mineral assemblages of Palaeogene foreland sediments, the Quebrada de los Colorados Formation (QLC), cropping out in the northern Calchaquí Valley (NW Argentina, Fig. 1). This 1400-metre-thick continental succession constitutes the first filling of the Andean foreland basin, recently defined as a broken foreland (del Papa et al., 2013).

The main objectives of this study are twofold: 1) link the variations in clay mineral assemblages across a north-south transect

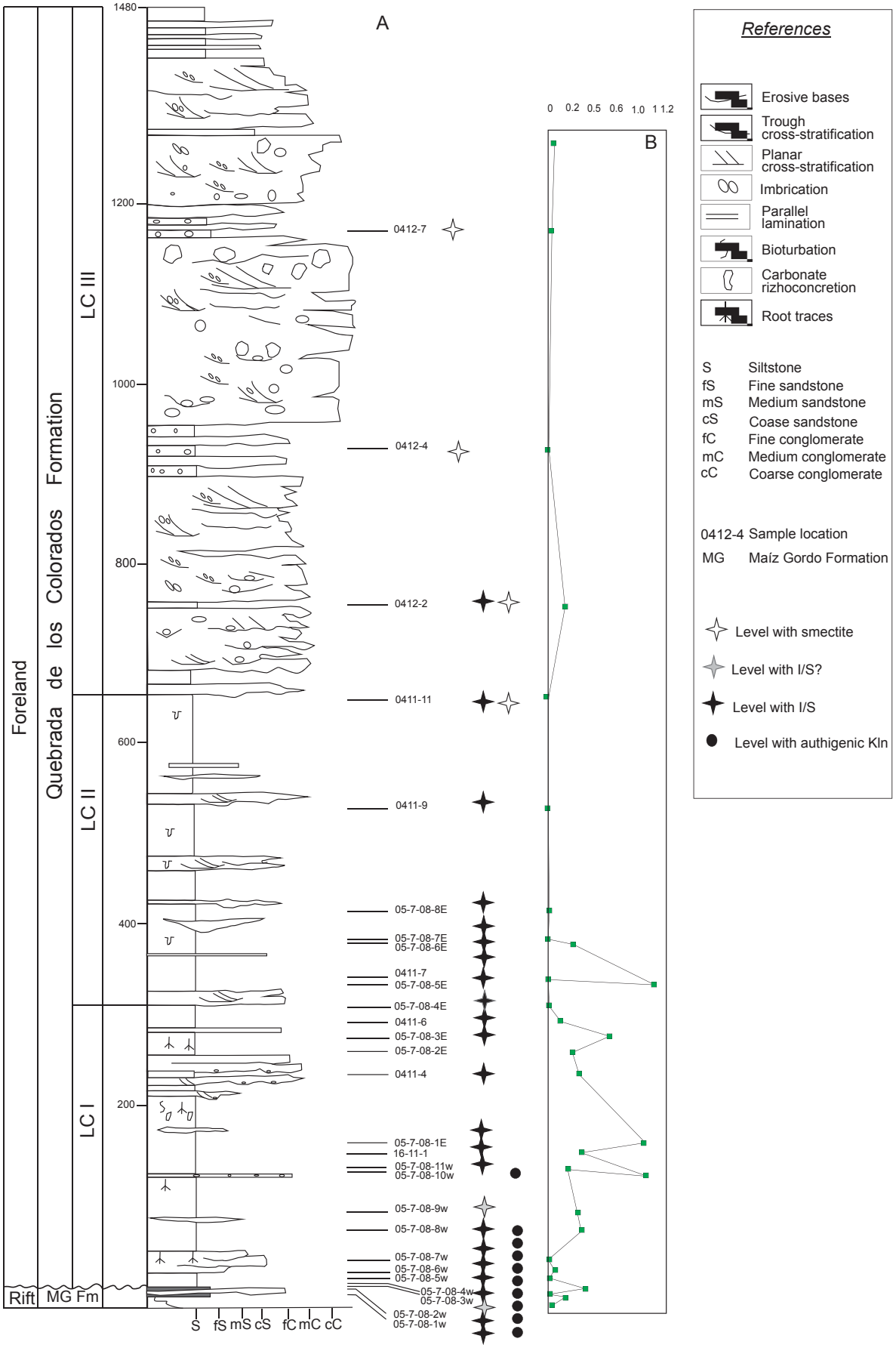

Fig. 2. A) Stratigraphic log of the Palaeogene Saladillo sequences. Levels containing authigenic kaolinite, mixed-layer I/S, and smectite are indicated; B) Variation of Kln/Ms ratios along the stratigraphic column.

with variations in factors contemporaneous with sedimentation, such as tectonism, source area lithology, and local palaeoenvironmental conditions; and 2) unravel parameters controlling the contrasting patterns in the diagenetic evolution of the I/S mixed-layers of the foreland sediments using X-ray diffraction, SEM, and TEM in conjunction with sedimentary facies analyses. We aim to test the usefulness of clay mineral analysis in the understanding of complex Andean foreland basin evolution.

2. Geological framework

The Central Andes of Northwestern Argentina comprise five morphotectonic provinces (Puna Plateau, Eastern Cordillera, Subandean belt, Santa Bárbara system, and Sierras Pampeanas), each characterized by different tectonic styles and stratigraphic successions (Jordan et al., 1983); all of them resulted from the subduction of the Farallón/Nazca Plate beneath the South American Plate. The Calchaquí Valley is located in the Eastern Cordillera, a morphotectonic unit characterized by thick-skinned tectonics comprising a basement of Neoproterozoic–early Cambrian very low-grade metamorphic rocks and a sedimentary cover grouped into two main basins (Mon and Salfity, 1995; Allmendinger et al., 1983): 1) Upper Cretaceous to lower Eocene sandstones and minor limestone rocks of the Salta rift basin (Salfity and Marquillas, 1994; Marquillas et al., 2005) and 2) middle Eocene to Pliocene sandstones and conglomerates of the Payogastilla Group, representing the infilling of the foreland basin (Díaz and Malizzia, 1983; del Papa et al., 2004) (Fig. 1A). An angular unconformity separates the sediments of the rift basin infilling from the overlying Payogastilla Group, whose basal unit is the Quebrada de Los Colorados Formation (QLC Formation) (Díaz et al., 1987). This foreland basin has had a complex evolution since its formation in the middle Eocene (Hongn et al., 2007, 2011), as evidenced by the spatial distribution of depocentres, the wedge-shaped basin geometry, as well as intrabasinal faults controlling sedimentation and local source areas (Hongn et al., 2007; Payrola et al., 2009; Hongn et al., 2011).

Table 1
Mineralogical composition of the clay fraction in the Saladillo area based on XRD results. Semi-quantitative abundances of clay minerals and Kln/Ms ratios were calculated employing MIF factors proposed by Moore and Reynolds (1997). The type of I/S mixed-layer corresponds to those identified by deconvolution methods (see also Fig. 3). Samples in bold were studied by SEM and/or TEM.

Sequence	Sample	Clay mineralogy	I/S	Kln/Ms
QLC LC III	0412-7			0.00
	0412-4			0.00
	0412-2		R0, R1	0.11
QLC LC II	0411-11		R1, R0	0.00
	0411-9			0.00
	5-7-08-8E			0.00
	5-7-08-7E		R0, R1	0.00
	5-7-08-6E			0.28
	0411-7			0.00
	5-7-08-5E			1.13
QLC LC I	5-7-08-4E		R0, R1, R3	0.03
	0411-6		R1, R3, R0	0.12
	5-7-08-3E			0.62
	5-7-08-2E			0.31
	0411-4		R1, R0	0.33
	5-7-08-1E		R1	1.08
	1611-1		R1, R0	0.33
	5-7-08-11W			0.18
	5-7-08-10W			1.00
	5-7-08-9W	?		0.30
	5-7-08-8W			0.36
	5-7-08-7W			0.02
	5-7-08-6W		R1, R3	0.07
	5-7-08-5W			0.06
	5-7-08-4W			0.35
	5-7-08-3W	?		0.04
Maíz Gordo F.	5-7-08-2W			0.19
	5-7-08-1W		R3, R1	0.07

Our study focuses on the northern Calchaquí Valley (Saladillo and Cerro Bayo areas), a N–S striking depression bounded by upward-convergent reverse faults defining a triangle geometry (Calchaquí and Toro Muerto; Marrett et al., 1994; Fig. 1B). In this area, the QLC Formation consists of a 1400-m-thick upward-thickening and -coarsening continental succession of claystones, siltstones, sandstones, and conglomerates, representing sedimentation in fluvial-alluvial plains and alluvial fan settings (del Papa et al., 2013) (Fig. 2). Based on unconformities and abrupt changes in the sedimentary facies patterns, three main depositional sequences have been recognized in the Saladillo and Cerro Bayo areas: Los Colorados I, Los Colorados II, and Los Colorados III (LC I, LC II, and LC III respectively, Figs. 1 and 2) (del Papa et al., 2005; Hongn et al., 2007). The basal strata of the study sections correspond to the Maíz Gordo Formation (post-rift sequence of the Salta Group), which are overlain in angular unconformity by the QLC Formation, constituting the first filling of the foreland (Díaz and Malizzia, 1983; Figs. 1 and 2).

Considerable evidence of synorogenic deposition was identified at Saladillo by Hongn et al. (2007) based on structural and sedimentary facies analyses. These authors concluded that folding of the Saladillo syncline was partially contemporaneous with deposition of the QLC Formation; furthermore, the east-vergent Toro Muerto fault was also active during sedimentation (Hongn et al., 2007). Deformation events, and consequently fault activity, also took place in the Neogene and Quaternary, as documented by the intersection of fold axes (see Fig. 1 in Hongn et al., 2007) and by the dilatant zones controlling the eruption of the Los Gemelos and Saladillo Quaternary fault-related volcanic centres (Marrett et al., 1994).

3. Sampling and analytical techniques

Samples for X-ray diffraction (XRD) analysis of bulk samples and clay–mineral analysis of the <2 μm sub-fraction were collected in Saladillo and Cerro Bayo in the northern Calchaquí Valley (Fig. 1). At the Saladillo site, sampling covered fined-grained layers (claystones, siltstones, and sandy siltstone beds) of the LC I, LC II, and LC III sequences, representing sedimentation in an alluvial plain setting (26 samples). In addition, with the aim of understanding the burial history of the sequences cropping out in this area, the sampling included not only the sediments of the foreland basin (QLC), but also the underlying Maíz Gordo Formation (post-rift sequences). Samples selected according to XRD data were studied with scanning electron microscopy (SEM) and transmission electron microscopy (TEM). Eight of these samples correspond to the different steps of the smectite → I/S → illite transformation and one (5-7-08-10W) corresponds to a kaolinite-rich bed. Additionally, five samples of the basal fine-grained QLC beds were gathered at a control point 15 km to the south (Cerro Bayo). Standard petrographic analyses were carried out on all samples to determine mineralogical composition and texture. Thin sections of pelites were obtained after resin impregnation (DICAST LY 554) in order to prevent break down. The mineralogical composition of 33 powdered samples was determined by X-ray diffraction (XRD) using a Philips PW1050 diffractometer (INGEIS). Clay sub-samples (<2 μm) were prepared in accordance with the guidelines of Moore and Reynolds (1997). Details about sample preparation and diagram interpretation can be found in Do Campo et al. (2010). In addition, the I/S mixed-layers in these sediments were studied in depth in ten of the samples with an XRD step scan, using a PANalytical X'Pert Pro diffractometer (CuKα radiation, 45 kV, 40 mA) equipped with an X'Celerator solid-state linear detector (Departament of Mineralogy and Petrology, University of Granada). These XRD traces were deconvoluted with the MacDiff software.

The mineral intensity factors of Moore and Reynolds (1997) were employed to estimate the relative abundances of micas, kaolinite, and chlorite. The ratio of kaolinite and mica (Kln/Ms) abundances, proposed as a palaeoclimatic index by Chamley (1989), was then calculated. The semi-quantitative analysis of I/S mixed-layers and smectite was performed selecting their reflections around 14–17°2θ; peaks in the low-angle region were only employed when the others were absent (Moore and Reynolds, 1997). Furthermore, the textures and mineralogy of selected claystones and siltstones were examined by SEM employing polished thin sections using back-scattered electron imaging and X-ray dispersive (EDS) analysis with a ZEISS DSM 950 scanning electron microscope (Scientific Instrument Centre, University of Granada, CIC). Unprocessed chips of the same samples, coated with 50 Å of carbon, were examined with a FEI, Quanta 400 environmental-pressure scanning electron microscope using secondary electrons (CEAMA) (see Do Campo et al., 2010 for image acquisition and chemical analysis methods). To determine the morphology and composition of individual I/S mixed-layer particles, we studied four samples by TEM with a Philips CM-20 working at 200 kV (University of Granada) on scattered powders on gold grids using the same methods as described in Drief and Nieto (2000). Chemical analyses were performed with an EDAX microanalysis system. Atomic concentration ratios were converted into formulae according to stoichiometry. Accordingly, the structural formulae of I/S mixed-layers was calculated on the basis of 22 negative charges $O_{10}(OH)_2$. The tetrahedral sites were filled with Al to make Si + Al = 4 and the remaining Al was assigned to octhaedral positions. All the iron was assumed to be ferric and all Mg was assigned to octahedral sites.

4. Results

4.1. Clay mineralogy

The mineralogy of the clay fraction for the Saladillo and Cerro Bayo areas is summarized in Tables 1 and 2, respectively. At Saladillo, the Maíz Gordo Formation comprises illite-muscovite, I/S

Table 2
Mineralogical composition of the clay fraction in the Cerro Bayo area based on XRD results. Semi-quantitative abundances of clay minerals and Kln/Ms ratios were calculated employing MIF factors proposed by Moore and Reynolds (1997).

Sequence	Sample	Clay mineralogy	Kln/Ms
QLC LC I	412-20		0.10
	412-16		0.06
	412-14		0.00
	412-12		0.10
	412-1b		0.10

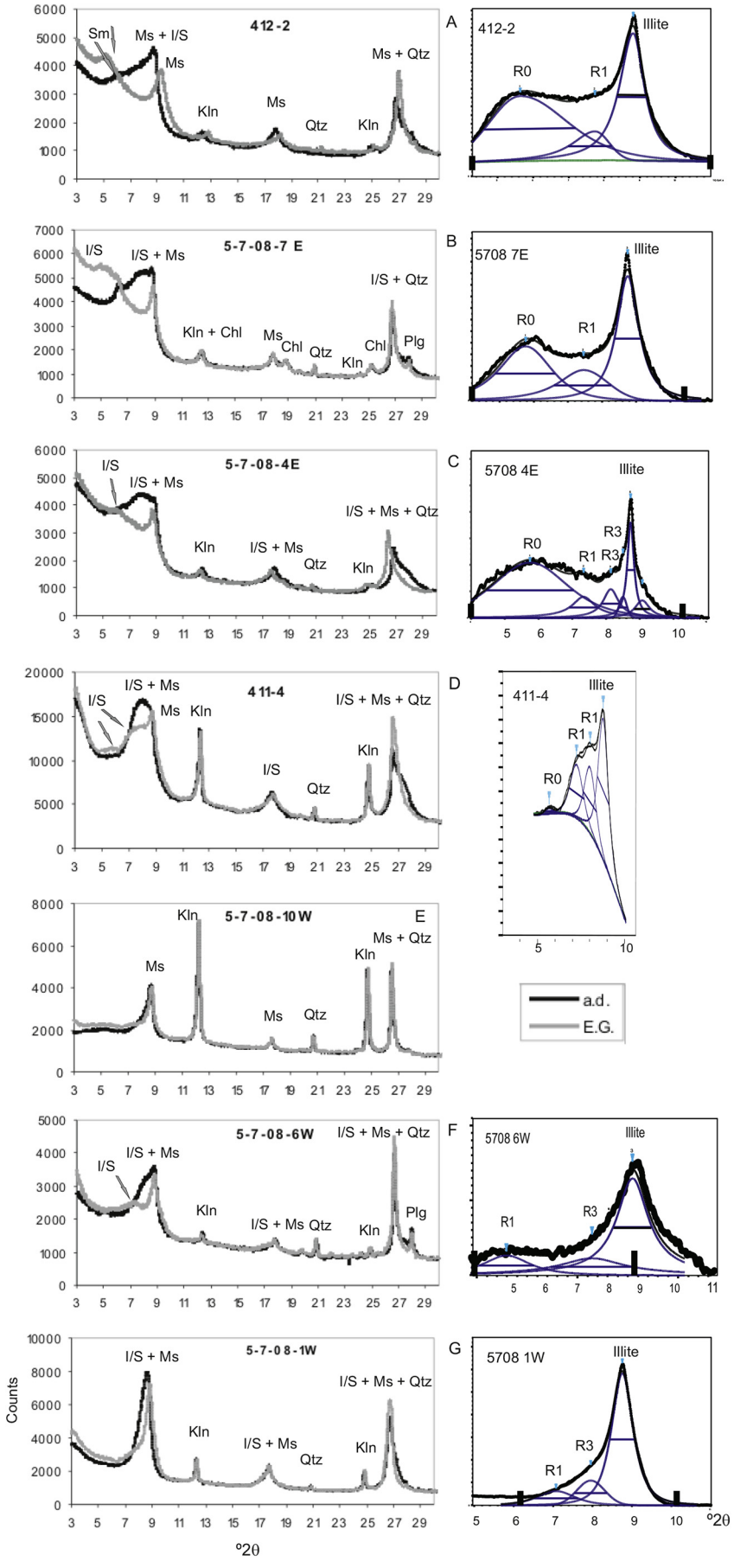
412-2
Sm
Ms + I/S
Ms
Kln
Ms
Qtz
Kln
Ms + Qtz
A
412-2
Illite
R0
R1
5-7-08-7 E
I/S
I/S + Ms
Kln + Chl
Ms
Chl
Qtz
Kln
Chl
Plg
I/S + Qtz
B
5708 7E
Illite
R0
R1
5-7-08-4E
I/S
I/S + Ms
Kln
I/S + Ms
Qtz
Kln
I/S + Ms + Qtz
C
5708 4E
Illite
R0
R1
R3
411-4
I/S
I/S + Ms
Ms
Kln
I/S
Qtz
Kln
I/S + Ms + Qtz
D
411-4
Illite
R0
R1
R1
5-7-08-10W
Kln
Ms
Ms
Qtz
Kln
Ms + Qtz
E
a.d.
E.G.
5-7-08-6W
I/S
I/S + Ms
Kln
I/S + Ms Qtz
Kln
Plg
I/S + Ms + Qtz
F
5708 6W
Illite
R1
R3
5-7-08-1W
I/S + Ms
Kln
I/S + Ms
Qtz
Kln
I/S + Ms + Qtz
G
5708 1W
Illite
R1
R3
Counts
°2θ
°2θ

mixed-layers, and subordinate kaolinite (Fig. 3G). Deconvolution discriminates between I/S R3 (≅ 85–90% illite layers) and subordinate I/S R1 (Fig. 3G right). The lower beds of the overlying QLC Formation have a similar composition to the Maíz Gordo Formation. However, less than 50 m upsection, the dominant I/S form is R1, with subordinate R3 type (Fig. 3F). Then, from the middle of LC I (around 150 m from the base of the unit), the I/S mixed-layers are mainly ordered to weakly ordered R1, in general with minor R0 (Table 1, Fig. 3D right). For the same sample (411-4), a deconvolution performed in the zone of 16–17°2θ (not shown) revealed two peaks (at 5.31 and 5.16) that indicate illite contents of around 65% and 85% in R1 I/S respectively, according to the Moore and Reynolds' method (1997). To the top of the LC I sequence, deconvolution performed on two samples indicates complex mixtures of R0, R1, and R3 (Table 1, Fig. 3C). In addition, a sharp increase in kaolinite abundance is recorded towards the middle of LC I, reaching Kln/Ms peak values of 1.00 and 1.08 in two strata, one of which does not contain I/S or smectite (Figs. 3E and 2B). Around 50 m upsection, an abrupt decrease in kaolinite abundance and in the Kln/Ms ratio is seen in LC I, linked with the reappearance of I/S mixed-layers (Table 1). The first pelitic bed of LC II has a sharp increase in kaolinite abundance and Kln/Ms ratio compared to the underlying LC I levels; however, this is an exception because kaolinite is absent or very scarce in the overlying pelitic beds in LC II (Fig. 2B). In LC II, I/S are represented by weakly ordered R1 associated with I/S R0 (Table 1), which becomes the dominant form 380 m from the base of the unit (Fig. 3B). Then, a pelitic bed in sequence LC III (ca. 750 m from the unit base) contains abundant micas and smectite, together with I/S mixed-layers and subordinate kaolinite. Deconvolution indicates that the latter do not have a unique component; in contrast, discrimination between I/S R0 and subordinate I/S R1 was possible (Fig. 3A right). Finally, 930 m from the base of LC III, I/S is absent, whereas smectite abundance increases (Table 1).

In contrast, the basal beds in sequence LCI at the Cerro Bayo site contain abundant smectite and micas, subordinate kaolinite and chlorite, and no I/S mixed-layers (Table 2).

4.2. SEM and TEM

Five samples from the QLC Formation were studied under SEM, and three were selected for TEM-AEM analysis. In addition, two samples from the Maíz Gordo Formation were observed under SEM and TEM respectively.

According to XRD data, the siltstone of the Maíz Gordo Formation contains illite-rich I/S R3 (Fig. 4A and B, and Table 3), which frequently occurs in the matrix in close association with illite grains of similar length that could only be distinguished from each other by their composition (Fig. 4A and B, EDS 7/1 to 7/10 in Table 3). Nevertheless, the structural formulae calculated from EDS microanalyses do not always permit a clear differentiation between I/S and illite-like compositions. Likewise, the detrital or authigenic nature of the illite grains could not be irrefutably determined at the SEM scale. This siltstone matrix also contains kaolinite, which in some cases is intermixed with tiny illite grains having extremely Fe–Mg-poor and Al-rich compositions (Fig. 4C, EDS 5-2 in Table 3) that probably resulted from kaolinite layers interleaved at a small scale. Kaolinite also partly replaces large mica laths, showing displacive precipitation along the cleavage planes, leading to 'fanning' along the edges of the mica flakes (Fig. 4A) (De Ros, 1998; Arostegui et al., 2001). However, kaolinization of micas is only partial and relatively fresh micas are also common (Fig. 4C). Kaolinite has also replaced tabular idiomorphic grains (Fig. 4B, lower left), and is the main component of pelitic lithoclasts up to 200 μm long (Fig. 4A).

TEM examination of clay-sized material from the uppermost mudstone of the Maíz Gordo Formation and the basal bed of the QLC revealed dominant thin, irregular platy particles less than 1 μm in diameter, with scarcer thick platy particles more than 3 μm long. AEM microanalyses evidence compositions that could correspond to illite rich-I/S or illite, which is in agreement with the I/S R3 (85–90% illite layers) indicated by XRD analysis. Illite grains depicting markedly Fe–Mg-poor and Al-rich compositions is another feature in common with the underlying siltstone 5-7-08-1W (Table 3).

In the lower beds of the QLC (Kln/Ms = 0.07), kaolinite occurs as an alteration product of K-feldspar, with platy and rarely hair-like morphologies (Fig. 4D) or forming the rock matrix (Fig. 4E). Illitic phases, which according to microanalysis and XRD correspond to I/S, were also identified in the matrix or as an alteration product of plagioclase (Fig. 4D, upper left, EDS 5/4 in Table 3). Scarce quartz crystals showing embayments and skeletal forms, with I/S filling the voids, were identified in this sample. Dolomite and minor calcite cements are closely associated with clay minerals. Chips of sample 411-4 (sequence LC I) were observed in fresh cut under SEM (Fig. 4F); mixed-layer I/S occurs as delicate curled foils resembling the rose-like morphology of smectite grains from the southern basin (Do Campo et al., 2010), suggesting an authigenic origin.

In the fine sandstones from the middle of the LC I sequence (5-7-08-10W, Kln/Ms = 1), kaolinite mainly comprises rounded or subhedral pelitic lithoclasts up to 200 μm long, frequently in close association with dolomite (Fig. 5A,B,C and D) and less frequently with calcite (Fig. 5B and C). Kaolinite also replaces albite with embayments (Fig. 5A and C) or tabular idiomorphic grains (Fig. 5C); additionally, it seldom replaces detrital mica lamellae along with displacive precipitation along the edges of mica flakes (Fig. 5A). Very scarce I/S (Fig. 5D, EDS 1–8 in Table 3), not identified by XRD, is also present in the matrix. The silty sandstones from the upper part of sequences LC II show fresh plagioclase and K-feldspar clasts, as well as unaltered mica laths (Fig. 6A); the matrix is mainly composed of I/S mixed-layers and subordinate smectite (Fig. 6A), although tiny illite grains also occur. The basal strata of sequence LC III also have fresh plagioclase and K-feldspar clasts, as well as unaltered mica laths (Fig. 6B and C). In these levels, the matrix is mainly composed of smectite and micas, with subordinate kaolinite and I/S (Fig. 6C and D).

4.3. AEM-EDS results

Mixed-layer I/S cannot be differentiated from illite and smectite based on structural formulae alone because their respective compositional ranges overlap each other. Therefore, the assignment of each microanalysis to one phase or the other depends upon textural evidence (grain size, morphology) as well as the clay assemblage determined by XRD analyses. However, AEM-EDS analyses suggest the occurrence of subordinate phases not previously identified by XRD; for example, minor smectite along with R1 or R0 mixed-layer I/S in the upper strata of the Saladillo sequence. Therefore, assignment to one particular phase is subject to a significant error and consequently conclusions based on differentiation among single grains of the same sample could be circular. We

Fig. 3. Representative X-ray air-dried (a.d.) and ethylene-glycol (E.G.) solvated patterns of <2 m sub-samples. The right column shows decomposition of the low-angle region (obtained with MacDiff) of ethylene-glycol solvated patterns for samples containing I/S mixed-layers. A) QLC, LC III, sample 412-2. B) QLC, LC II, sample 5-7-08-7E. C) QLC, upper LC I, sample 5-7-08-4E. D and E), QLC, middle LC I sequence, samples 411-4 and 5-7-08-10W respectively. F) QLC, LC I sequence, sample 5-7-08-6W. G) Maíz Gordo Formation, sample 5-7-08-1W.

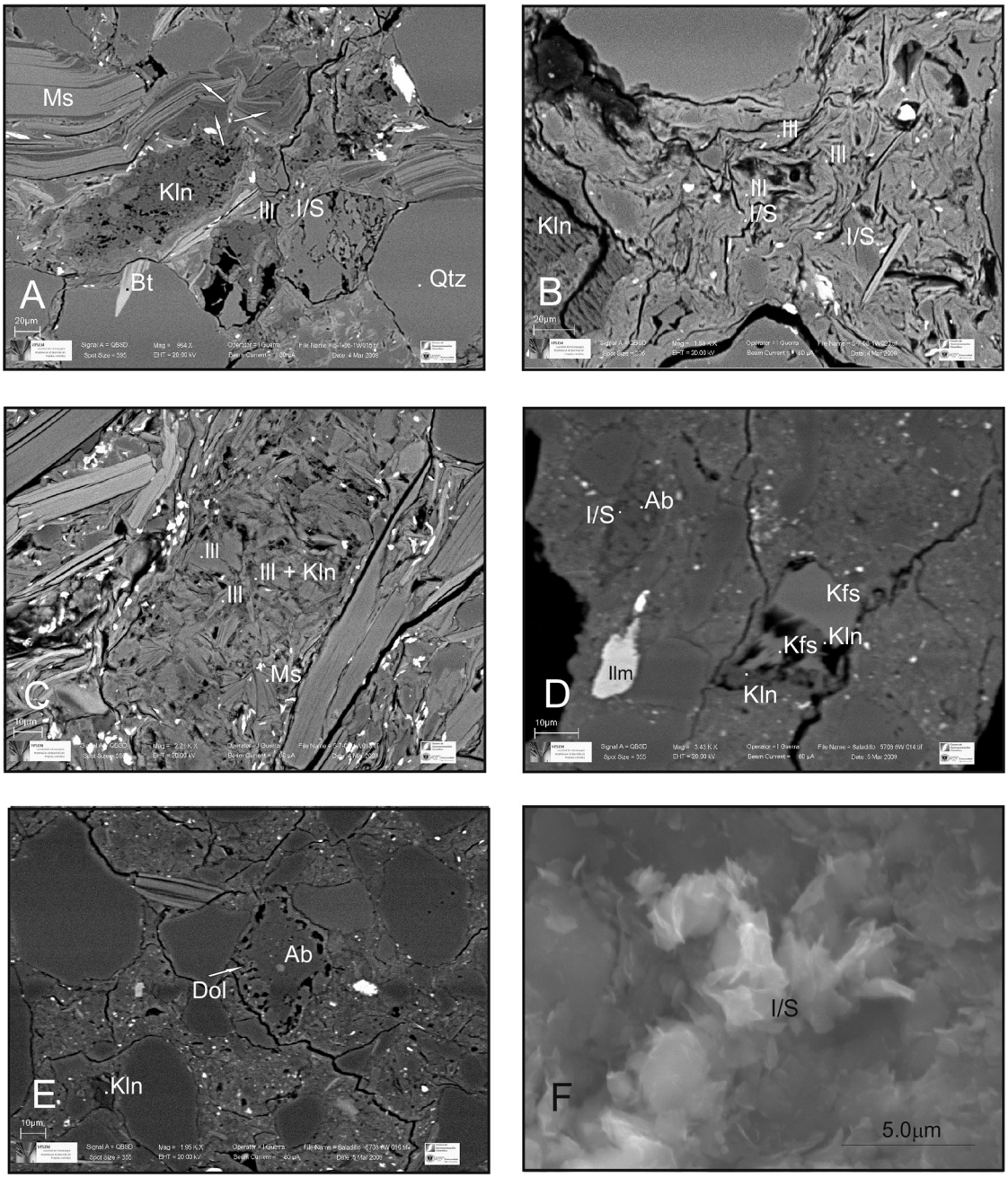

Fig. 4. BSE images A–C: sample 5-7-08-1W, Maíz Gordo Formation. A) Laths of detrital mica showing pseudomorphic replacement of the lamellae and additional displacive kaolinite precipitation between the cleavage planes (upper left), rounded detrital grain mainly composed of kaolinite (centre) and mixed-layer I/S in the matrix. B) Detrital mica lath associated with mixed-layer I/S in the matrix and tabular idiomorphic grain pseudomorphically replaced by kaolinite (lower left). C) Kaolinite intermixed with tiny illite grains in the matrix. D) Hairy kaolinite growing in a pore, rounded albite grain replaced by mixed-layer I/S in the borders (upper left) (sample 5-7-08-6W, LCI sequence). E) Dolomite rimming a detrital albite grain, kaolinite in the matrix (lower left) (5-7-08-6W). F) Secondary electron image showing mixed-layer I/S occurring as delicate curled foils (sample 411-4 sequence LC I). Abbreviations of minerals according to Kretz (1983) and updated by Whitney and Evans (2010).

address possible means to avoid this problem by examining the chemical compositions of mixed layers in the various samples based on their predominant I/S phase as determined by XRD analyses, including all the analysed grains, with the sole exception of obvious detrital micas. Accordingly, we first depict the composition of mixed layers sample by sample, but in the following discussion we have arranged them into three groups: smectite-I/S R0, I/S R1, and I/S R > 1. We are aware that these criteria increase the apparent compositional overlap among different phases, but we expect that general trends can be identified.

Mixed-layer I/S shows a broad compositional range with Si contents from 3.14 to 3.84 atoms per formula unit (apfu), a sum of interlayer charges from 0.24 to 0.81 apfu, and Fe + Mg contents from 0.00 to 0.83 apfu (Table 3). The Fe–Mg-poor and Al-rich I/S corresponds to the siltstones from the Maíz Gordo Formation and the overlying 5-7-08-3W (QLC, LC I sequence). Such anomalous Al-rich compositions are frequently accompanied by high octahedral occupancy and low interlayer charge, probably resulting from interlayered kaolinite at a small scale, which is in agreement with SEM observations (Fig. 4A and C). Consequently, such analyses,

Table 3
Representative structural formulae for I/S according to EDS and AEM data; predominant I/S type in each sample, according to XRD, is indicated. Analyses were normalized for 10 O and 2 (OH). Samples 411-4 and 1611-1 were analysed by AEM, the rest by EDS. *Analyses contaminated with kaolinite.

	I/S R3																																						
	5-7-08 1W																										5-7-08-2W							5-7-08-3W				
	1/4	2/7	2/8	3/4	4/1	4/5	5/2*	6/8	6/9	6/10	7/1	7/2	7/3	7/4	7/5	7/6	7/9	7/10	6/1	6/2	6/3	6/4	6/5	6/6	6/7	21*	23	2*	6*	9*	13*	18	2	3*	10	19	20
Si	3.28	3.24	3.41	3.38	3.26	3.20	3.14	3.28	3.29	3.30	3.23	3.25	3.27	3.29	3.28	3.25	3.26	3.24	3.23	3.20	3.24	3.26	3.24	3.25	3.30	3.40	3.38	3.47	3.30	3.26	3.34	3.52	3.43	3.26	3.51	3.26	3.41
A^{IIV}	0.72	0.76	0.59	0.62	0.74	0.80	0.86	0.72	0.71	0.70	0.77	0.75	0.73	0.71	0.72	0.75	0.74	0.76	0.77	0.80	0.76	0.74	0.76	0.75	0.70	0.60	0.62	0.53	0.70	0.74	0.66	0.48	0.57	0.74	0.49	0.74	0.59
Al^{VI}	1.62	1.65	1.67	1.47	1.57	1.54	2.00	1.59	1.57	1.56	1.58	1.62	1.56	1.57	1.73	1.74	1.55	1.56	1.64	1.63	1.55	1.54	1.60	1.58	1.62	1.92	1.58	1.99	2.06	1.83	2.10	1.52	1.77	1.94	1.85	1.56	1.53
Fe	0.22	0.20	0.19	0.30	0.24	0.29	0.00	0.23	0.26	0.25	0.24	0.22	0.24	0.25	0.20	0.17	0.24	0.23	0.21	0.21	0.28	0.28	0.25	0.23	0.22	0.04	0.27	0.00	0.00	0.07	0.00	0.18	0.10	0.00	0.14	0.32	0.37
Mg	0.16	0.13	0.17	0.20	0.20	0.21	0.00	0.21	0.17	0.19	0.20	0.17	0.19	0.18	0.08	0.10	0.18	0.19	0.14	0.12	0.23	0.23	0.16	0.19	0.16	0.11	0.25	0.00	0.00	0.16	0.00	0.37	0.16	0.14	0.00	0.27	0.25
Ti	0.03	0.05	0.02	0.01	0.04	0.03	0.00	0.04	0.03	0.04	0.03	0.03	0.05	0.04	0.00	0.02	0.07	0.07	0.04	0.06	0.00	0.02	0.04	0.04	0.05	0.00	0.00	0.00	0.00	0.00	0.00	0.00	0.00	0.00	0.00	0.00	0.00
$\sum$ oct.	2.02	2.02	2.05	1.99	2.06	2.07	2.00	2.06	2.03	2.04	2.05	2.04	2.03	2.05	2.01	2.02	2.04	2.05	2.03	2.03	2.06	2.07	2.05	2.05	2.04	2.06	2.09	1.99	2.06	2.06	2.10	2.07	2.03	2.08	1.99	2.15	2.15
K	0.79	0.69	0.55	0.85	0.69	0.71	0.84	0.62	0.67	0.61	0.72	0.69	0.64	0.64	0.70	0.72	0.69	0.69	0.71	0.69	0.77	0.74	0.68	0.65	0.63	0.53	0.55	0.57	0.50	0.61	0.37	0.41	0.64	0.65	0.54	0.57	0.40
Na	0.00	0.00	0.00	0.00	0.00	0.00	0.00	0.00	0.00	0.05	0.00	0.00	0.05	0.00	0.00	0.00	0.00	0.00	0.00	0.00	0.00	0.00	0.00	0.06	0.00	0.00	0.05	0.00	0.00	0.12	0.00	0.23	0.00	0.00	0.00	0.00	0.00
Ca	0.00	0.04	0.02	0.00	0.02	0.02	0.00	0.05	0.05	0.03	0.03	0.03	0.04	0.03	0.04	0.02	0.02	0.02	0.03	0.04	0.02	0.00	0.03	0.03	0.02	0.00	0.00	0.00	0.00	0.00	0.00	0.00	0.00	0.00	0.00	0.00	0.00
Σ int.	0.79	0.77	0.59	0.85	0.73	0.76	0.84	0.71	0.77	0.73	0.77	0.76	0.77	0.71	0.78	0.76	0.72	0.73	0.77	0.78	0.81	0.74	0.74	0.76	0.68	0.53	0.60	0.57	0.50	0.73	0.37	0.64	0.64	0.65	0.54	0.57	0.40
Al_{tot}	2.34	2.42	2.26	2.09	2.31	2.33	2.86	2.31	2.27	2.26	2.35	2.36	2.28	2.28	2.45	2.49	2.30	2.33	2.41	2.44	2.31	2.28	2.36	2.34	2.32	2.52	2.19	2.52	2.76	2.57	2.76	2.01	2.33	2.68	2.34	2.30	2.12
Fe + Mg	0.37	0.32	0.36	0.50	0.45	0.50	0.00	0.43	0.43	0.44	0.44	0.39	0.42	0.43	0.28	0.27	0.42	0.42	0.35	0.33	0.51	0.51	0.41	0.42	0.38	0.14	0.51	0.00	0.00	0.23	0.00	0.55	0.26	0.14	0.14	0.58	0.61

	I/S R1																																						
	5-7-08-6W										10W	1611-1													411-4													
	5/4	6/4	8/1	8/2	8/3	8/4	3	2/4	5/13	5/14	1/8	1	2	3	4	6	8	9	10	11	12	13	15	2	3	5	6	9	11	13	14	15	16	18	20	21	22
Si	3.56	3.53	3.45	3.53	3.56	3.58	3.65	3.36	3.57	3.55	3.55	3.45	3.80	3.55	3.58	3.81	3.61	3.47	3.84	3.61	3.27	3.45	3.52	3.41	3.45	3.56	3.45	3.32	3.57	3.56	3.67	3.46	3.38	3.42	3.64	3.41	3.41
A^{IIV}	0.44	0.47	0.55	0.47	0.44	0.42	0.35	0.64	0.43	0.45	0.45	0.55	0.20	0.45	0.42	0.19	0.39	0.53	0.16	0.39	0.73	0.55	0.48	0.59	0.55	0.44	0.55	0.68	0.43	0.44	0.33	0.54	0.62	0.58	0.36	0.59	0.59
Al^{VI}	1.63	1.37	1.38	1.38	1.41	1.41	1.45	1.45	1.32	1.36	1.57	1.61	1.60	1.80	1.61	1.57	1.56	1.59	1.63	1.46	1.40	1.57	1.50	1.63	1.68	1.72	1.66	1.56	1.66	1.72	1.70	1.71	1.74	1.59	1.63	1.58	1.94
Fe	0.08	0.37	0.37	0.36	0.35	0.31	0.26	0.29	0.37	0.33	0.27	0.18	0.12	0.04	0.23	0.14	0.23	0.19	0.12	0.21	0.52	0.19	0.18	0.23	0.14	0.21	0.12	0.26	0.19	0.19	0.12	0.17	0.17	0.21	0.16	0.19	0.03
Mg	0.36	0.24	0.25	0.25	0.25	0.22	0.24	0.24	0.27	0.28	0.15	0.28	0.28	0.18	0.23	0.31	0.26	0.28	0.29	0.35	0.23	0.33	0.33	0.26	0.31	0.21	0.30	0.28	0.24	0.19	0.23	0.19	0.23	0.26	0.23	0.30	0.16
Ti	0.00	0.03	0.04	0.03	0.00	0.05	0.03	0.02	0.03	0.04	0.02	0.00	0.00	0.00	0.00	0.00	0.00	0.00	0.00	0.02	0.00	0.02	0.04	0.00	0.00	0.00	0.00	0.00	0.00	0.00	0.00	0.00	0.00	0.00	0.00	0.00	0.00
$\sum$ oct.	2.07	2.01	2.04	2.02	2.00	1.98	1.98	2.00	2.00	2.01	2.01	2.07	2.00	2.01	2.06	2.02	2.05	2.07	2.04	2.04	2.15	2.11	2.05	2.12	2.14	2.14	2.08	2.11	2.09	2.10	2.05	2.08	2.14	2.06	2.01	2.08	2.13
K	0.11	0.50	0.58	0.56	0.46	0.55	0.52	0.72	0.54	0.55	0.23	0.44	0.19	0.28	0.23	0.12	0.26	0.35	0.21	0.26	0.37	0.26	0.35	0.38	0.31	0.24	0.46	0.47	0.29	0.21	0.12	0.31	0.24	0.33	0.23	0.35	0.12
Na	0.43	0.08	0.00	0.00	0.11	0.00	0.04	0.07	0.02	0.02	0.00	0.12	0.12	0.30	0.07	0.21	0.14	0.16	0.12	0.21	0.12	0.17	0.14	0.00	0.00	0.00	0.00	0.00	0.00	0.05	0.19	0.10	0.10	0.14	0.16	0.21	0.14
Ca	0.03	0.04	0.04	0.04	0.06	0.05	0.03	0.03	0.06	0.04	0.15	0.04	0.09	0.00	0.09	0.05	0.05	0.05	0.00	0.07	0.02	0.05	0.07	0.05	0.07	0.00	0.07	0.09	0.05	0.03	0.05	0.03	0.03	0.09	0.09	0.05	0.05
Σ int.	0.59	0.66	0.66	0.64	0.68	0.64	0.62	0.84	0.67	0.67	0.54	0.63	0.48	0.58	0.47	0.43	0.50	0.61	0.33	0.61	0.52	0.54	0.63	0.49	0.45	0.24	0.60	0.65	0.40	0.33	0.42	0.49	0.42	0.65	0.56	0.67	0.37
Al_{tot}	2.07	1.84	1.93	1.85	1.86	1.83	1.79	2.09	1.75	1.80	2.02	2.16	1.80	2.25	2.03	1.77	1.95	2.12	1.78	1.86	2.13	2.11	1.98	2.22	2.23	2.16	2.22	2.25	2.09	2.16	2.03	2.25	2.36	2.17	1.99	2.18	2.52
Fe + Mg	0.44	0.61	0.62	0.61	0.59	0.53	0.50	0.53	0.65	0.61	0.42	0.46	0.40	0.21	0.45	0.45	0.49	0.47	0.42	0.56	0.75	0.52	0.51	0.49	0.45	0.41	0.42	0.54	0.43	0.38	0.35	0.37	0.40	0.47	0.38	0.49	0.19

	I/S R1						I/S R0 − Sm																																	
	411-4						411-9																												412-2					
	23	24	25	27	29	31	3/9	4/3	4/4	4/7	2/3	2/4	6/12	8/13	9/16	9/17	1/3	1/4	1/5	1/8	1/10	2/4	2/8	2/12	3/2	3/4	3/5	2/7	3/4	4/1	4/2	4/3	4/4	5/1	5/2	5/5	6/5
Si	3.61	3.33	3.44	3.30	3.50	3.34	3.52	3.76	3.47	3.61	3.57	3.52	3.51	3.52	3.66	3.65	3.59	3.55	3.57	3.49	3.43	3.47	3.79	3.50	3.54	3.56	3.53	3.59	3.50	3.50	3.50	3.53	3.63	3.58	3.60	3.48	3.80
A^{IIV}	0.39	0.67	0.56	0.70	0.50	0.66	0.48	0.24	0.53	0.39	0.43	0.48	0.49	0.48	0.34	0.35	0.41	0.45	0.43	0.51	0.57	0.53	0.21	0.50	0.46	0.44	0.47	0.41	0.50	0.50	0.50	0.47	0.37	0.42	0.40	0.52	0.20
Al^{VI}	1.59	1.54	1.69	1.66	1.66	1.68	1.22	1.42	1.18	1.23	1.22	1.17	1.21	1.25	1.24	1.24	1.31	1.35	1.38	1.25	1.16	1.27	1.29	1.28	1.31	1.33	1.40	1.24	1.36	1.50	1.52	1.28	1.26	1.51	1.51	1.53	1.33
Fe	0.21	0.25	0.17	0.21	0.21	0.18	0.32	0.22	0.36	0.38	0.39	0.42	0.35	0.33	0.38	0.34	0.30	0.29	0.27	0.34	0.41	0.38	0.28	0.32	0.33	0.33	0.24	0.41	0.27	0.22	0.20	0.37	0.40	0.21	0.23	0.19	0.31
Mg	0.29	0.33	0.24	0.19	0.26	0.28	0.42	0.32	0.35	0.31	0.37	0.37	0.47	0.37	0.37	0.37	0.41	0.39	0.37	0.39	0.42	0.39	0.39	0.44	0.41	0.38	0.44	0.36	0.35	0.33	0.32	0.41	0.32	0.35	0.33	0.28	0.32
Ti	0.00	0.00	0.00	0.00	0.00	0.00	0.08	0.03	0.14	0.08	0.03	0.03	0.03	0.05	0.03	0.06	0.03	0.02	0.02	0.06	0.04	0.02	0.02	0.03	0.02	0.02	0.02	0.03	0.03	0.03	0.03	0.02	0.02	0.00	0.00	0.01	0.03
$\sum$ oct.	2.09	2.12	2.11	2.06	2.13	2.13	2.04	1.99	2.03	2.00	2.01	1.99	2.07	2.00	2.03	2.00	2.04	2.04	2.04	2.04	2.04	2.05	1.99	2.08	2.07	2.07	2.10	2.04	2.01	2.08	2.07	2.08	2.01	2.08	2.07	2.01	2.00
K	0.14	0.37	0.24	0.51	0.16	0.37	0.50	0.40	0.46	0.49	0.43	0.50	0.44	0.52	0.44	0.42	0.48	0.52	0.46	0.48	0.49	0.43	0.34	0.49	0.48	0.46	0.42	0.50	0.61	0.44	0.43	0.49	0.48	0.30	0.30	0.65	0.41
Na	0.17	0.12	0.10	0.05	0.16	0.11	0.00	0.00	0.00	0.00	0.03	0.05	0.04	0.03	0.01	0.09	0.00	0.00	0.00	0.00	0.15	0.09	0.08	0.00	0.00	0.00	0.06	0.00	0.00	0.00	0.04	0.00	0.05	0.00	0.00	0.06	0.00
Ca	0.05	0.07	0.07	0.07	0.03	0.04	0.10	0.08	0.10	0.06	0.14	0.15	0.12	0.13	0.07	0.07	0.10	0.09	0.09	0.13	0.10	0.11	0.10	0.10	0.07	0.07	0.07	0.07	0.09	0.07	0.06	0.06	0.06	0.12	0.12	0.02	0.04
Σ int.	0.42	0.63	0.49	0.70	0.38	0.54	0.71	0.56	0.65	0.62	0.74	0.85	0.71	0.82	0.59	0.64	0.67	0.69	0.65	0.74	0.84	0.74	0.61	0.68	0.62	0.61	0.60	0.64	0.79	0.58	0.58	0.62	0.64	0.54	0.53	0.75	0.50
Al_{tot}	1.98	2.22	2.25	2.35	2.16	2.34	1.70	1.65	1.70	1.62	1.65	1.65	1.70	1.73	1.58	1.59	1.72	1.80	1.81	1.76	1.73	1.80	1.50	1.78	1.77	1.77	1.87	1.65	1.86	2.00	2.02	1.75	1.63	1.93	1.91	2.05	1.54
Fe + Mg	0.50	0.58	0.42	0.40	0.47	0.46	0.74	0.54	0.71	0.69	0.76	0.79	0.82	0.70	0.75	0.70	0.71	0.68	0.64	0.73	0.83	0.77	0.67	0.76	0.74	0.72	0.68	0.77	0.62	0.56	0.52	0.78	0.72	0.56	0.56	0.47	0.63

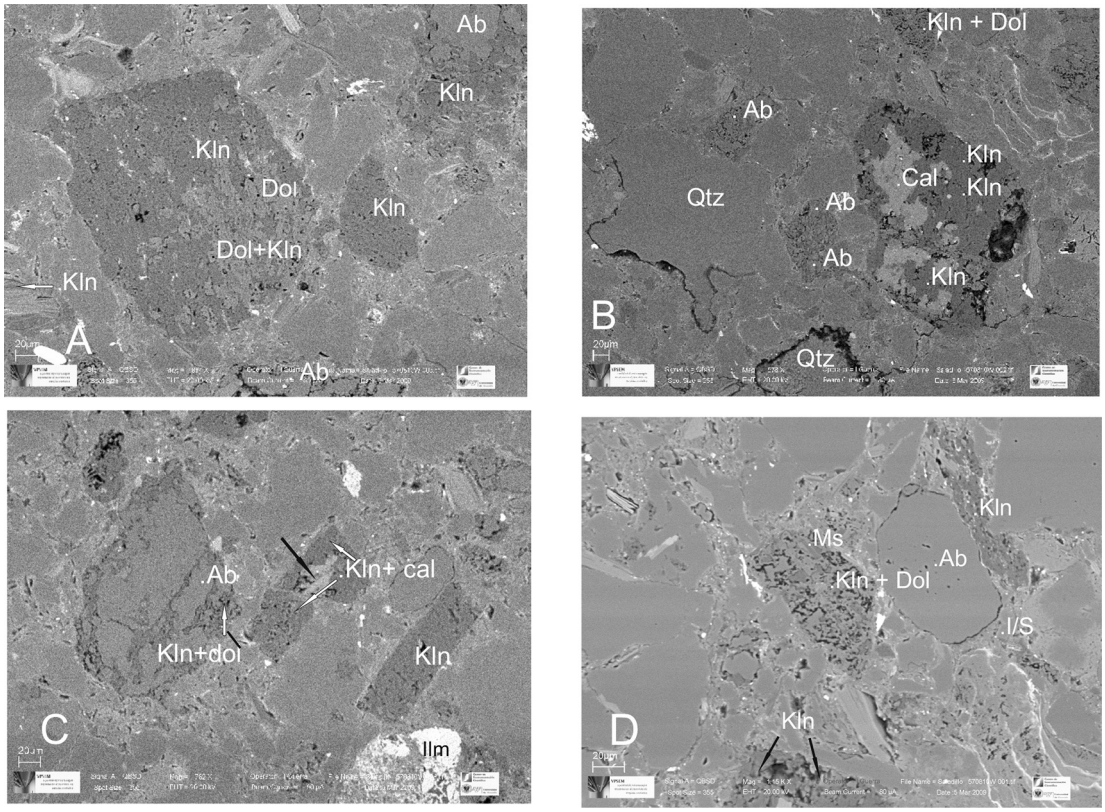

Fig. 5. BSE images A–D: Kaolinite occurring in different textural sites in sample 5-7-08-10W (LC I sequence). As subhedral or rounded pelitic lithoclasts composed entirely of kaolinite (A centre right), or of kaolinite in close association with dolomite (A, centre, B upper right, C centre left, D centre), and less frequently with calcite (B: centre; C: white arrows, impure calcite: black arrow), forming the matrix (A, D), replacing tabular idiomorphic grains (C, lower right), replacing albite crystals with embayments (A, upper right); less frequently, kaolinite appears as a pseudomorphic replacement of detrital mica lamellae (A, white arrow). This sample also contains albite grains without evidence of alteration (D centre) and subordinate I/S in the matrix (D centre).

identified with an asterisk in Table 3, will not be considered in the discussion below. On the other hand, Fe + Mg contents of over 0.77 apfu probably reflect contamination with a ferromagnesian silicate.

Mixed-layer I/S is widely scattered in the Si–Fe + Mg diagram (Fig. 7A); however, variations along a hypothetical phengite vector are not significant. At least in part, the data scattering may derive from a significant Fe^{+3} content and the Al by Si substitution due to the smectitic component.

As can be seen in the plots (Fig. 7B and C), when the samples are grouped according to their predominant I/S phase, the compositional fields of the three groups partially overlap.

Even though the compositional range for all the elements is wide, clear differences in their trends can be noted in Table 3 and Fig. 7B. First, as the type of predominant I/S phase, from I/S R3, to R1, and then to R0, varies gradually from bottom to top, a significant change obviously occurs in the chemical composition of mixed-layer I/S with depth.

Significant chemical changes from the top (smectite – R0 I/S) to the bottom (R3 I/S – illite) can be summed up as follows:

- Si decreases from 3.8 to 3.2
- Al increases from 1.5 to 2.49
- Mg drops from 0.47 to ~0.1
- Ca decreases from 0.15 to 0

Fig. 7C shows that a wide variation in these chemical parameters exists within each group; nonetheless, a consistent variational trend from R0 to R3 (with R1 being intermediate) is also evident.

5. Discussion

5.1. Factors affecting variations in the Kln/Ms ratio

On a global scale, the Early Eocene has been recognized as a period of optimal climate (EECO; Zachos et al., 1992; Hollis et al., 2005); since then, the climate has become progressively more arid. In the study area, in the southern Central Andes (and particularly in the Puna region), warm and humid conditions during the Eocene are supported by palaeosols in the Maíz Gordo Formation (White et al., 2010). Subsequently, well-documented aridity has persisted from the Oligocene to the Present (Vandervoort et al., 1995; Clarke, 2006; Strecker et al., 2007). Accordingly, a decrease in the Kln/Ms ratio, compatible with progressively lower hydrolyzing conditions, should be observed (Chamley, 1989). However, this is not the trend at the Saladillo site (Fig. 2 and Table 1), where kaolinite abundance as well as Kln/Ms ratios vary sharply and in an irregular zigzag pattern (Fig. 2 B). Nonetheless, as mentioned above, kaolinite can only be employed in palaeoclimatic reconstruction when it comes from mature and mineralogically differentiated soils developed in the same sedimentary cycle (Thiry, 2000). In the studied sediments, textural evidence indicates that kaolinite has two predominant origins, diagenetic and inherited from previous sedimentary cycles; kaolinite that formed coevally with QLC sedimentation by intense weathering of bedrocks is subordinate or absent. Diagenetic origin is attested by the occurrence of tabular idiomorphic grains entirely replaced by kaolinite (Fig. 5A and C) in beds with high Kln/Ms ratios. In these beds, kaolinite also occurs as the main component of reworked fine-grained rocks (Fig. 5A).

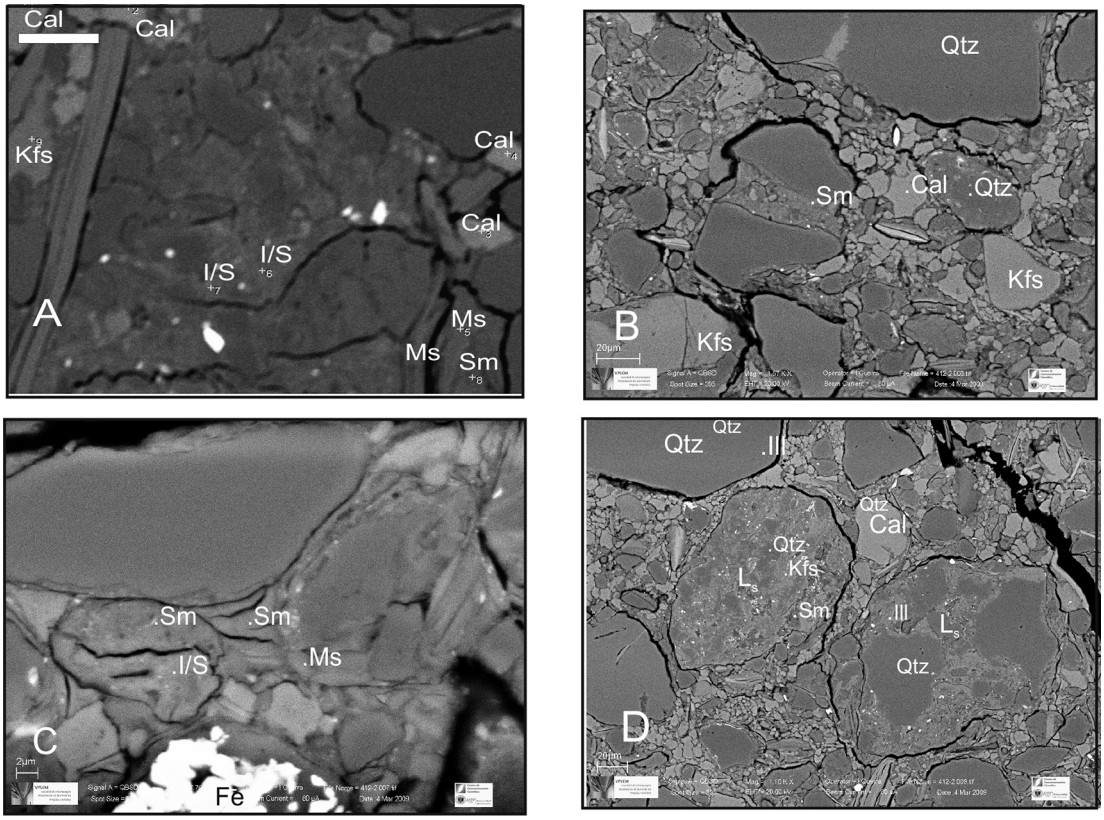

Fig. 6. A) Unaltered mica laths and K-feldspar clasts in a matrix composed of I/S and subordinate smectite in sample 411-9 (upper part of LC II sequence). Micritic calcite occurs as anhedral clasts but also mixed with clay minerals in the matrix; B–D: Sample 412-2 (LC III sequence). B) Unaltered grains of K-feldspar, abundant micritic calcite clasts, and minor smectite in the matrix. C) Matrix detail comprising smectite, tiny detrital micas, and subordinate I/S. D) Lithoclasts of probable sedimentary origin mainly composed of quartz, K-feldspar, plus a matrix of smectite and illite.

Taking into account that palaeosol beds, almost smectite-free, dominated by kaolinite and detrital micas, are characteristic of the Maíz Gordo Formation (Do Campo et al., 2007; White et al., 2010), these kaolinite-rich fine-grained lithoclasts are most likely a consequence of the unroofing of this unit. This interpretation is in agreement with the angular unconformity relation between Maíz Gordo and LC I. Therefore, the sharp increase in kaolinite content in several beds from the LC I and LC II sequences (Fig. 2) cannot be interpreted in terms of palaeoclimatic changes but instead to the reworking of palaeosol levels from the Maíz Gordo Formation. At the same time, such smectite-free parent material could explain the near lack of I/S (only EDS 1–8 correspond to this phase in sample 5-7-08-10W) and of smectite in the levels with the highest kaolinite abundances. In contrast with the northern Calchaquí Valley, where kaolinite is moderately abundant, towards the south kaolinite is very scarce or absent (Do Campo et al., 2010). This is in agreement with a source area dominated by very low-grade metamorphic rocks and granites, as also deduced from provenance studies (Do Campo et al., 2010).

5.2. Diagenetic changes

The vertical variation from smectite at the top to I/S R0 to R1, and then R3 at the base of the QLC in the northernmost Calchaquí Valley is a typical diagenetic burial pattern (Merriman and Frey, 1999 and references therein). Moreover, authigenic kaolinite was documented by SEM images from the base of the Saladillo section (Fig. 4A and D) up to circa 150 m upsection (Fig. 5B–D). Furthermore, I/S R3 with 85–90% illite layers, as well as diagenetic kaolinite, have also been recorded in the underlying Maíz Gordo Formation. It is highly probable that smectite would have been the common precursor of all the different I/S stages in these sediments, with their progressive differences throughout the sedimentary column being a consequence of different degrees of diagenetic evolution.

Using a combination of EDS and AEM, we have been able to obtain a representative set of good-quality analyses with a stoichiometry that is coherent with the smectite and illite possible extreme compositions. The most relevant chemical changes from the top (smectite - R0 I/S) to the bottom (R3 I/S – illite) are: (1) a decrease in Si to Al exchange in the tetrahedral layer (Fig. 7B), and (2) a decrease in Ca contents (Table 3). This compositional trend is expected for a diagenetic smectite to illite transformation and has been described in other studies (Nieto et al., 1996; Árkai, 2002).

I/S formation from a smectitic precursor is controlled by several variables, primarily temperature, original lithology, and K availability (Abid et al., 2004; Arostegui et al., 2006). The temperatures estimated for the transformation from I/S R0 to R1 in siliciclastic sediments of different basins are 75–120 °C (Hoffman and Hower, 1979; Pollastro, 1993; Schegg and Leu, 1996), whereas the transition temperature from I/S R1 to ordered I/S R3 in sediments older than 5 Ma would be approximately 175 °C (Pollastro, 1993). Late diagenetic conditions are also suggested by the occurrence of authigenic kaolinite in the lowest strata of the Saladillo site because kaolinite consumption due to prograde reactions in the realm of burial diagenesis or in geothermal systems occurs at temperatures of around 200 °C (Boles and Franks, 1979; Merriman and Frey, 1999; Giorgetti et al., 2000).

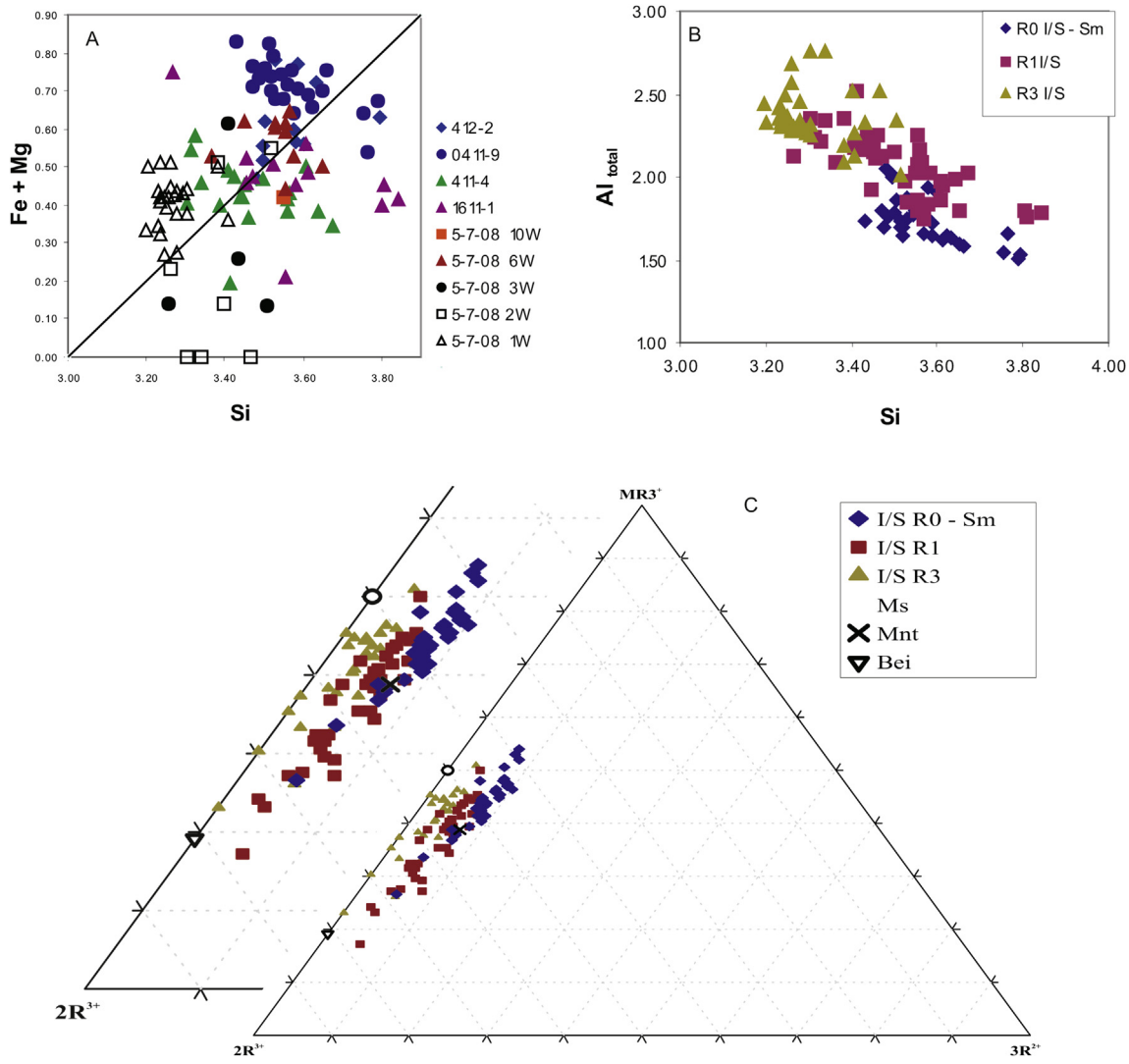

Fig. 7. Compositional plots for I/S microanalyses. A) sample by sample, B and C) samples grouped according to the dominant type of mixed-layer I/S as determined by XRD analysis (Table 2): R0 I/S-Sm, R1 I/S or R3 I/S. A) Si − Fe + Mg plot. B) Si − total Al. C) triangular $MR3^{+}$-$2R^{3+}$-$3R^{2+}$ diagram (Velde, 1985), theoretical compositions of muscovite, montmorillonite (Mnt) and beidellite (Bei) are included for comparison purposes. $MR3^{+}$: $(Na^{+} + K^{+} + 2Ca^{2+})$, $2R^{3+}$: (total Al + Fe^{+3} − Int charge)/2, $3R^{2+}$: $(Fe^{+2} + Mg^{2+})/3$ according to Arroyo (2010).

In contrast, the clay mineral assemblages of foreland sediments cropping out at Cerro Bayo, only 15 km to the south, are dominated by smectite to the bottom of the sequence (Table 2), which indicates that they were only affected by early diagenesis. Furthermore, in central parts of the Calchaquí Valley (Tin Tin Basin), previously described by Do Campo et al. (2010), the basal levels contain smectite and no I/S mixed-layers.

In the study area, the maximum sedimentary thickness preserved above the basal deposits of the QLC Formation is approximately of 3000 m, and so this value can be reasonably assumed as a minimum for the burial depths of the QLC Formation. However, burial depth could have been even lower for the Saladillo site as less sedimentary thickness is recorded in this area, which is in agreement with data indicating early exhumation as deduced from the ~10 Ma Negra Muerta andesite lava flow overlying the 13 Ma Nevado de Acay monzonite (Haschke et al., 2005; Riller et al., 2001). In addition, an intermediate to slightly low geothermal gradient is likely for the northern and southern basin since foreland basins are regarded as hypothermal basins, depicting lower geothermal gradients and heat flows than average values (Dorsey et al., 1988; Allen and Allen, 2005). Therefore, the late diagenesis attested for the sediments from the base of the study section up to the middle of sequence LC I could not be explained by the estimated burial conditions. This diagenetic grade also represents a significant contrast with the early diagenetic conditions inferred for equivalent levels cropping out towards the south (i.e. Cerro Bayo and Tin Tin basin). The northern Calchaquí Valley is bounded by the Toro Muerto and Calchaquí reverse faults, which are only 4 km apart in the Saladillo area, whereas sampling points are less than 1 km from the fault planes. These faults were active at several stages during the Cenozoic, as evidenced by the syndepositional deformation features preserved in the Palaeogene sediments studied, the Neogene refolding of the Eocene folds, the related Quaternary volcanic centres, and historical earthquakes (Marrett et al., 1994; Hongn et al., 2007). These faults may have promoted the circulation of deep fluids that would have favoured smectite illitization in the proximity of the fault planes. The lack of I/S mixed-layers in the basal beds of QLC in other areas of the basin, including a control point only 15 km to the south (Table 2), demonstrates that the attainment of late diagenesis for these successions is exceptional.

This heterogeneous pattern of diagenetic evolution could be related with the fact pointed out by Quinlan (1988) that the palaeogeothermal gradient in foreland basins could be heavily influenced by large-scale fluid flow drived by different mechanisms. According to a hydrological model formulated by Garven and Freeze (1984), in foreland basins, meteoric water enters the system near the foothill and is channelled along permeability boundaries by the gravitational effect of the sloping water table. Instead, it was suggested that the overburden pressure related with the emplacement of orogenic thrust sheets squeezes fluid from the sediments of the overridden margin, driving it to the foreland basin (Oliver, 1986). In the case of the northern Calchaquí Valley, the occurrence of permeable sandstone and conglomeratic sandstone layers interbedded with siltstone levels may have facilitated fluid flow in the proximity of the faults. Stress could also have acted as a driving force that gathered burial diagenesis at the R3 mixed-layer I/S stage in these continental sediments.

The link between areas depicting enhanced I/S evolution and the activity of fluids in faulted zones has been mentioned previously for different basins (Uysal et al., 2000; Abid and Hesse, 2007).

In the case of the Bowen Basin (Queensland, Australia), contrasting stages of I/S evolution were identified between its northern and southern areas (Uysal et al., 2000). This contrast could not be explained by differences in maximum burial as the northern area, showing enhanced I/S evolution, does not correspond with the basin depocentre. On the other hand, the northern area of the Bowen Basin was subjected to extensional tectonic activity during the Late Triassic. Consequently, these authors postulated that faults and permeable fracture zones facilitated deep penetration of meteoric fluids; later, fluids carried heat upwards by convection, generating local geothermal anomalies that would be responsible for the intensified I/S evolution in the northern parts of the Bowen Basin (Uysal et al., 2000).

In addition, Abid and Hesse (2007) have recently postulated the key role of fluids channelled by faults as directly involved in diagenetic reactions to explain anomalous areas of enhanced illitization in the offshore Jeanne d'Arc Basin of Canada. This study found that cross plots of %I in I/S against organic-matter maturation (R_0) are generally linear, supporting temperature control for illitization. However, these authors found a lack of linear correlation between %I in I/S and (R_0) in the Trans-Basinal Fault zone and part of the Outer Ridge Complex, areas characterized by numerous faults. Illitization is particularly rapid in the 30–70% illite range, causing step-shaped depth profiles that support the supposition that illitization was not temperature-driven (Abid and Hesse, 2007).

Two recent cases have also demonstrated the decisive role of faults in diagenetic and very low-temperature metamorphic processes in the Canadian Appalachians of Nova Scotia. In the late Palaeozoic St. Mary's Basin, the pattern of Kubler index and I/S mixed-layers indicates a temperature increase towards the Chedabucto Fault, produced by two superposed events, the first at high-anchizone–lower greenschist-facies conditions and the second at retrograde–diagenetic conditions (Abad et al., 2010). In the Silurian-Devonian Arisaig Group, where no correlation exists between the metamorphic conditions and either the stratigraphic depth or the strain values measured by phyllosilicate orientation analyses, the metamorphic grade generally increases towards the Hollow Fault, and is highest in samples within a 1 km corridor from the fault surface (Abad et al., 2012).

The data in our study do not allow us to conclude with certainty whether fluids were directly involved in smectite illitization in foreland sediments at the Saladillo site, or whether they acted as a heat carrier circulating through permeable sandstone and conglomeratic sandstone layers interbedded with siltstone beds.

This study demonstrates that the analysis of clay mineral assemblages beyond palaeoclimatic reconstructions is a valuable tool to understand the complex evolution of foreland basins. Moreover, the connection between areas with enhanced diagenetic evolution and fault activity could be a key to search for oil-generating strata in active basins that, due to shallow burial or low geothermal gradients, do not entirely reach organic matter maturation.

6. Conclusions

We were able to determine the origin of clay minerals for a sedimentary succession employing XRD in conjunction with SEM images. In this succession, kaolinite cannot be used as a palaeoclimatic proxy; in contrast, sharp increases in kaolinite abundance reflect a source area episodically dominated by kaolinite-rich palaeosols that were reworked into the foreland basin.

On the other hand, the authigenic kaolinite plus R3 illite/smectite mixed-layer assemblage in the basal 150 m at the Saladillo site indicates late diagenesis. The diagenetic grade indicated by clay minerals is exceptional for a sequence that underwent shallow burial (~3000 m) in a low geothermal gradient basin. The faults that bounded the northern Calchaquí Valley (Toro Muerto and Calchaquí reverse faults), active during the deposition of the QLC Formation, may have promoted the circulation of hot, deep fluids that favoured smectite illitization. Furthermore, the upward convergence of the Toro Muerto and Calchaquí faults could have promoted a stress concentration, particularly in narrower zones of the valley such as those surveyed in this study. This stress could have acted as a driving force that promoted burial diagenesis at the R3 mixed-layered I/S stage in these continental sediments.

Acknowledgements

This work was partially financed by CONICET - PIP 489 and ANCyT - PICT 0407 grants and Research Project CGL2011-30153-C02-01 (Spanish Ministry of Science). The stay of M. Do Campo at the University of Granada and the field work of Fernando Nieto in Argentina were supported by AECI project A/7712/07. The authors are grateful to G. Giorgetti and an anonymous reviewer for their valuable and constructive comments. We also thank Christine Laurin for revising the English text.

References

Abad, I., Brendan Murphy, J., Nieto, F., Gutiérrez-Alonso, G., 2010. Diagenesis to metamorphism transition in an episutural basin: the late Paleozoic St. Mary's Basin, Nova Scotia, Canada. Can. J. Earth Sci. 47, 121–135.

Abad, I., Nieto, F., Gutiérrez-Alonso, G., Brendan Murphy, J., Braid, J.A., Rodríguez-Navarro, A.B., 2012. Fluid-driven low-grade metamorphism in polydeformed rocks of Avalonia (Arisaig Group, Nova Scotia, Canada). Swiss J. Geosci. 105, 283–297.

Abid, I.A., Hesse, R., 2007. Illitizing fluids as precursors of hydrocarbon migration along transfer and boundary faults of the Jeanne d'Arc Basin offshore Newfoundland, Canada. Mar. Petrol. Geol. 24, 237–245.

Abid, I.A., Hesse, R., Harper, J.D., 2004. Variations in mixed-layer illite/smectite diagenesis in the rift and post-rift sediments of the Jeanne d'Arc Basin, Grand Banks offshore Newfoundland, Canada. Can. J. Earth Sci. 41, 401–429.

Adatte, T., Keller, G., Stinnesbeck, W., 2002. Late Cretaceous to early Paleocene climate and sea-level fluctuations: the Tunisian record. Palaeogeogr. Palaeoclimatol. Palaeoecol. 178, 165–196.

Allen, P.A., Allen, J.R., 2005. Basin Analysis: Principles and Applications. Blackwell Scientific Publications, Cambridge, p. 451.

Allmendinger, R., Ramos, V., Jordan, T., Palma, R., Isacks, B.L., 1983. Paleogeography and Andean structural geometry, northwest Argentina. Tectonics 2, 1–16.

Árkai, P., 2002. Phyllosilicates in very low-grade metamorphism: transformation to micas. In: Mottana, A., Sassi, F.P., Thompson Jr., J.B., Guggenheim, S. (Eds.), Micas: Crystal Chemistry and Metamorphic Petrology, Reviews in Mineralogy & Geochemistry, vol. 46. Mineralogical Society of America, Washington, D.C, pp. 463–478.

Arostegui, J., Irabien, M.J., Nieto, F., 2001. Microtextures and the origin of muscovite-kaolinite intergrowths in sandstones of the Utrillas Formation, Basque Cantabrian Basin, Spain. Clays Clay Minerals 49, 529–539.

Arostegui, J., Sangüesa, F.J., Nieto, F., Uriarte, J.A., 2006. Thermal models and clay diagenesis in the Tertiary-Cretaceous sediments of the Alava block (Basque-Cantabrian basin, Spain). Clay Miner. 41, 791–809.
Arroyo, X., 2010. Evolución de las esmectitas e interestratificados I/S en la serie carbonatada del Cretácico Superior del Bloque Alavés (Ph.D. dissertation). In: Implicaciones sobre el mecanismo de illitización durante la diagénesis. Universidad del País Vasco, p. 252.
Bevins, R.E., White, S.C., Robinson, D., 1996. The South Wales Coalifield: low-grade metamorphism in a foreland basin setting? Geol. Mag. 133, 739–749.
Boles, J.R., Franks, S.G., 1979. Clay diagenesis in Wilcox sandstones of Southwest Texas: implication of smectite diagenesis on sandstone cementation. J. Sedmentary Petrology 49, 55–70.
Do Campo, del Papa, C., Jiménez-Millán, J., Nieto, F., 2007. Clay mineral assemblages and analcime formation in a Palaeogene fluvial-lacustrine sequence (Maiz Gordo Formation) from Northwestern Argentina. Sediment. Geol. 201, 56–74.
Chamley, H., 1989. Clay Sedimentology. Springer Verlag, Berlin, p. 623.
Clarke, J.D., 2006. Antiquity of aridity in the Chilean Atacama Desert. Geomorphology 73, 101–114.
Collo, G., Dávila, F.M., Nóbile, J., Astini, R.A., Gehrels, G., 2011. Clay mineralogy and thermal history of the Neogene Vinchina Basin, central Andes of Argentina: analysis of factors controlling the heating conditions. Tectonics 30, TC4012. http://dx.doi.org/10.1029/2010TC002841.
De Ros, L.F., 1998. Heterogeneous generation and evolution of diagenetic quartzarenites in the Silurian-Devonian Fumas Formation of the Paran Basin, southern Brazil. Sediment. Geol. 116, 99–128.
del Papa, C., Hongn, F., Petrinovic, I., Domínguez, R., 2004. Evidencias de deformación pre-miocena media asociada al antepaís andino en la Cordillera Oriental (24°35′ S - 66°12′ O). Asoc. Geol. Argent. Rev. 59, 506–509.
del Papa, C., Hongn, F., Mon, R., Powell, J., Petrinovic, I., 2005. Stratigraphy and syndepositional structures of the basal foreland deposits in the northern Valle Calchaquí, NW Argentina. In: VI International Symposium on Andean Geodynamics, Barcelona (Spain), pp. 215–217.
del Papa, C., Hongn, F., Powell, J., Payrola, P., Do Campo, M., Strecker, M.P., Petrinovic, I., Schmitt, A., Pereyra, R., 2013. Middle Eocene-Oligocene broken foreland evolution in the Andean Calchaqui Valley, NW Argentina: insights from stratigraphic, structural, and provenance studies. Basin Res. 25, 574–593.
Dera, G., Pellenard, P., Neige, P., Deconinck, J.-F., Pucéat, E., Dommergues, J.-L., 2009. Distribution of clay minerals in Early Jurassic Peritethyan seas: palaeoclimatic significance inferred from multiproxy comparisons. Palaeogeogr. Palaeoclimatol. Palaeoecol. 271, 39–51.
Díaz, J.I., Malizzia, D.C., 1983. Estudio geológico y sedimentológico del Terciario superior del Valle Calchaquí (Departamento de San Carlos, Prov. De Salta). Boletín Sedimentol. 2, 8–28.
Díaz, J., Malizzia, D., Bossi, G., 1987. Análisis estratigráfico del Grupo Payogastilla. In: X Congreso Geológico Argentino, vol. 2, pp. 113–116. Tucumán (Argentina).
Do Campo, M., Nieto, F., del Papa, C., Hongn, F., 2008. Composition of mixed-layered illite/smectite in a continental Eocene succession (Quebrada de los Colorados Formation, Salta Province, Argentina). SEM-SEA, Macla 9, 85–86.
Do Campo, M., del Papa, C., Nieto, F., Hongn, F., Petrinovic, I., 2010. Integrated analysis for constraining palaeoclimatic and volcanic influences on clay–mineral assemblages in orogenic basins (Palaeogene Andean foreland, Northwestern Argentina). Sediment. Geol. 228, 98–112.
Dorsey, R.J., Buchovecky, E.J., Lundberg, N., 1988. Clay mineralogy of Pliocene-Pleistocene mudstones, eastern Taiwan: combined effects of burial diagenesis and provenance unroofing. Geology 16, 944–947.
Drief, A., Nieto, F., 2000. Chemical composition of smectites formed in clastic sediments. Implications for the smectite-illite transformation. Clay Miner. 35, 665–678.
Fagel, N., Boski, T., Likhoshway, L., Oberhaensli, H., 2003. Late Quaternary clay mineral record in Central Lake Baikal (Academician Ridge, Siberia). Palaeogeogr. Palaeoclimatol. Palaeoecol. 193, 159–179.
Fesharaki, O., García-Romero, E., Cuevas-González, J., López-Martínez, N., 2007. Clay mineral genesis and chemical evolution in the Miocene sediments of Somosaguas, Madrid Basin, Spain. Clay Miner. 42, 187–201.
Garven, G., Freeze, R.A., 1984. Theoretical analysis of the role of groundwater flow in the genesis of stratabound ore deposits. I. Mathematical and numerical model. Am. J. Sci. 284, 1085–1124.
Giorgetti, G., Mata, M.P., Peacor, D.R., 2000. TEM study of the mechanism of transformation of detrital kaolinite and muscovite to illite/smectite in sediments of the Salton Sea Geothermal Field. Eur. J. Mineral. 12, 923–934.
Haschke, M., Deeken, A., Insel, N., Sobel, E., Grove, M., Schmitt, A.K., 2005. Growth pattern of the Andean Puna plateau constrained by apatite fission track, apatite (U-Th)/He, K-feldspar $^{40}Ar/^{39}Ar$, and zircon U-Pb geochronology. In: VI International Symposium on Andean Geodynamics (Barcelona), pp. 360–363.
Hoffman, J., Hower, J., 1979. Clay mineral Assemblages as Low Grade Metamorphic Geothermometers: Application to the Thrust Faulted Disturbed Belt of Montana, U. S. A. Society of Economic Paleontologists and Mineralogists, pp. 55–79. Special Publication 26.
Hollis, C.J., Dickens, G.R., Field, B.D., Jones, C.M., Strong, C.P., 2005. The Paleocene–Eocene transition at Mead Stream, New Zealand: a southern Pacific record of early Cenozoic global change. Palaeogeogr. Palaeoclimatol. Palaeoecol. 215, 313–343.
Hongn, F., del Papa, C.E., Powell, J., Petrinovic, I.A., Mon, R., Deraco, V., 2007. Middle Eocene deformation and sedimentation in the Puna-Eastern Cordillera transition (23°–26°S): control by preexisting heterogeneities on the pattern of inicial Andean shortening. Geology 35, 271–274.
Hongn, F., del Papa, C., Powell, J., Payrola, P., Petrinovic, I., Mon, R., 2011. Fragmented Paleogene foreland basin in the Valles Calchaquíes, NW of Argentina. In: Salfity, J.A., Marquillas, R.A. (Eds.), Cenozoic Geology of the Central Andes of Argentina. SCS Publisher, Salta, pp. 189–209.
Jordan, T., Isacks, B.L., Allmendinger, R.W., Brewer, J.A., Ramos, V.A., Ando, C.J., 1983. Andean tectonics related to geometry of the subduted Nazca plate. Geol. Soc. Am. Bull. 94, 341–361.
Marquillas, R., del Papa, C., Sabino, I., 2005. Sedimentary aspects and paleoenvironmental evolution of a rift basin: Salta Group (Cretaceous-Paleogene), northwestern Argentina. Int. J. Earth Sci. 94, 94–113.
Marrett, R.A., Allmendiger, R.W., Alonso, R.N., Drake, R.E., 1994. Late Cenozoic tectonic evolution of the Puna plateau and adjacent foreland, norwestern Argentine Andes. J. South Am. Earth Sci. 7, 179–208.
Merriman, R.J., Frey, M., 1999. Patterns of very low-grade metamorphism in metapelitic rocks. In: Frey, M., Robinson, D. (Eds.), Low-grade Metamorphism. Blackwell Science Limited, London, pp. 61–107.
Merriman, R.J., Peacor, D.R., 1999. Very low-grade metapelites: mineralogy microfabrics and measuring reaction progress. In: Frey, M., Robinson, D. (Eds.), Low-grade Metamorphism. Blackwell Science, Oxford, pp. 10–60.
Mon, R., Salfity, J.A., 1995. Tectonic evolution of the Andesof northern Argentina. In: Tankard, A.J., Suarez Soruco, R., Welsink, H.J. (Eds.), Petroleum Basins of South America, American Association of Petroleum Geologists, Mem, vol. 62, pp. 269–283.
Moore, D.M., Reynolds, R.C., 1997. X-ray Diffraction and the Identification and Analysis of Clay Minerals. Oxford University Press, Oxford, p. 378.
Net, L.I., Alonso, M.S., Limarino, C.O., 2002. Source rock and environmental control on clay mineral associations, Lower Section of Paganzo Group (Carboniferous), Northwest Argentina. Sediment. Geol. 152, 183–199.
Nieto, F., Ortega-Huertas, M., Peacor, D.R., Arostegui, J., 1996. Evolution of illite/smectite from early diagenesis through incipient metamorphism in sediments of the Basque-Cantabrian Basin. Clays Clay Minerals 44, 304–323.
Oliver, J., 1986. Fluids expelled tectonically from orogenic belts: their role in hydrocarbon migration and other geologic phenomena. Geology 14, 99–102.
Payrola Bosio, P.A., Powell, J., del Papa, C., Hongn, F., 2009. Middle Eocene deformation-sedimentation in the Luracatao Valley: tracking the beginning of the foreland basin of Northwestern Argentina. J. S. Am. Earth Sci. 28, 142–154.
Pollastro, R.M., 1993. Considerations and applications of the illite/smectite geothermometer in hydrocarbon-bearing rocks of Miocene to Mississippian age. Clays Clay Minerals 41, 119–133.
Quinlan, G., 1988. The thermal signatures of tectonic environments. In: Nisbet, E.G., Fowler, C.M.R. (Eds.), Short Course on Heat, Metamorphism and Tectonics. Mineralogical Association of Canada.
Riller, U., Petrinovic, I., Ramelow, J., Strecker, M., Onken, O., 2001. Late Cenozoic tectonism, collapse caldera and plateau formation in the Central Andes. Earth Planet. Sci. Lett. 188, 299–311. http://dx.doi.org/10.1016/S0012-821X(01)00333-8.
Saèz, A., Inglès, M., Cabrera, L., de las Heras, A., 2003. Tectonic–palaeoenvironmental forcing of clay–mineral assemblages in nonmarine settings: the Oligocene–Miocene as Pontes Basin (Spain). Sediment. Geol. 159, 305–324.
Salfity, J.A., Marquillas, R.A., 1994. Tectonic and sedimentary evolution of the Cretaceous-Eocene Salta Group Basin, Argentina. In: Salfity, J.A. (Ed.), Cretaceous Tectonics of the Andes, Earth Evolution Sciences. Friedr. Vieweg & Sohn, pp. 266–315.
Schegg, R., Leu, W., 1996. Clay mineral diagenesis and thermal history of the Thonex Well, Western Swiss Molasse Basin. Clays Clay Minerals 44, 693–705.
Strecker, M.R., Alonso, R., Bookhagen, B., Carrapa, B., Hilley, G.E., Sobel, E.R., Trauth, M.H., 2007. Tectonics and climate of the Southern Central Andes. Annu. Rev. Earth Planet. Sci. 35, 747–787.
Suresh, N., Ghosh, S.K., Kumar, R., Sangode, S.J., 2004. Clay–mineral distribution patterns in late Neogene fluvial sediments of the Subathu sub-basin, central sector of Himalayan foreland basin: Implications for provenance and climate. Sediment. Geol. 163, 265–278.
Thiry, M., 2000. Palaeoclimatic interpretation of clay minerals in marine deposits: an outlook from the continental origin. Earth-Sci. Rev. 49, 201–221.
Uysal, I.T., Glikson, M., Golding, S.D., Audsley, F., 2000. The thermal history of the Bowen Basin, Queensland, Australia: Vitrinite reflectance and clay mineralogy of Late Permian coal measures. Tectonophysics 323, 105–129.
Vandervoort, D.S., Jordan, T.E., Zeitler, P.K., Alonso, R., 1995. Chronology of internal drainage development and uplift, southern Puna plateau, Argentine central Andes. Geology 23, 145–148.
Velde, B., 1985. Clay Minerals a Physico-chemical Explanation of Their Occurrence. Elsevier, Amsterdan, p. 427.
White, T., del Papa, C., Rodriguez Brizuela, R., 2010. Paleosol-based paleoclimate reconstructions of late Paleocene through middle Eocene Argentina. In: 18th International Sedimentological Congress, (Mendoza), p. 910.
Whitney, D.L., Evans, B.W., 2010. Abbreviations for names of rock-forming minerals. Am. Mineral. 95, 185–187.
Zachos, J.C., Breza, J.R., Wise, S.W., 1992. Early Oligocene ice-sheet expansion on Antarctica: stable isotope and sedimentological evidence from Kerguelen Plateau, southern Indian Ocean. Geology 20, 569–573.